Int. J. Electrochem. Sci., 8 **(2013)** 8097 - 8114

International Journal of
ELECTROCHEMICAL
SCIENCE
www.electrochemsci.org

A Comparative Study of Ionic Conductivity, Translational Diffusion, Molecular Motion, and Physicochemical Properties in Lithium Bis(trifluoromethanesulfonyl)imide-Doped 1-Methyl-3-pentyl- and 1,2-Dimethyl-3-pentyl-substituted Imidazolium-Based Ionic Liquids

Yi-Jan Lin[1], *Lin Hao*[2], *Yuan-Chung Lin*[3], *Chung-Wen Kuo*[4], *Pin-Rong Chen*[5], *Tzi-Yi Wu*[5,*], *I-Wen Sun*[2,*]

[1] Graduate Institute of Natural Products and Center of Excellence for Environmental Medicine, Kaohsiung Medical University, Kaohsiung 807, Taiwan
[2] Department of Chemistry, National Cheng Kung University, Tainan 70101, Taiwan
[3] Institute of Environmental Engineering, National Sun Yat-Sen University, Kaohsiung 804, Taiwan
[4] Department of Chemical and Materials Engineering, National Kaohsiung University of Applied Sciences, Kaohsiung 80778, Taiwan
[5] Department of Chemical and Materials Engineering, National Yunlin University of Science and Technology, Yunlin 64002, Taiwan, ROC
[*]E-mail: wuty@yuntech.edu.tw, iwsun@mail.ncku.edu.tw

Received: 3 April 2013 / *Accepted:* 9 May 2013 / *Published:* 1 June 2013

The ionic conductivity, translational diffusion, molecular motion, and physicochemical properties of ionic liquids (ILs) and lithium bis(trifluoromethanesulfonyl)imide (LiTFSI)-doped ILs with two different imidazolium cations (1-methyl-3-pentylimidazolium $[MPI]^+$ and 1,2-dimethyl-3-pentyl-imidazolium $[DMPI]^+$) are characterized. Self-diffusion coefficients *D* for the anion and the cation are measured by pulsed field gradient spin echo NMR (PGSE-NMR), the measured ion diffusion coefficients, viscosities, and ionic conductivity follow the Vogel-Tammann-Fulcher (VTF) equation for the temperature dependencies, and the best-fit parameters are determined. LiTFSI-doped [MPI][TFSI] shows a NOE signal between Li^+ and MPI^+ and a broad Li peak was observed in HOESY spectra, whereas there is no NOE signal in LiTFSI-doped [DMPI][TFSI], demonstrating that one additional methyl group at the C-2 position in the $DMPI^+$ may prevent Li^+ to be closed to $DMPI^+$ via steric hindrance.

Keywords: Ionic liquid electrolyte, ionic conductivity, spin−lattice relaxation times, heteronuclear overhauser effect spectroscopy, lithium ion transference number

1. INTRODUCTION

During the past decade, ionic liquid is one of the current topics that attracts the attention of many researchers [1-12]. Due to an almost unlimited number of potential combinations of cations and anions, these salts are in a liquid state below 100 ˚C. Ionic liquids (ILs) have attracted great interests of researchers due to their superior properties, including negligible volatility, nonflammability, high chemical and thermal stability, high ionic conductivity and electrochemical stability [13-16], and they have been widely used, make them very attractive candidates as electrolytes in rechargeable lithium batteries [17-20], electrochemical sensor [21-37], solar cells [38-43], and fuel cell [44].

Recently, it has been reported that ionic liquids based electrolyte in lithium ion battery show good electrochemical stability and nonflammability. For instance, LiTFSI-doped *N*-butyl-*N*-ethylpyrrolidinium bis(trifluoromethanesulfonyl) imide (PYR24TFSI) shows a better stability in time toward lithium metal electrodes than the previously investigated imidazolium-based systems and also has a wider electrochemical stability window [45]. Thus, there is an interest to investigate the influence of Li salt addition also on other properties of lithium salt-doped ionic liquids. The translational (or self-) diffusion coefficient (D) and spin−lattice relaxation time (T_1) of a liquid are two of the most important physical parameters for probing solution interactions, pulsed gradient spin echo (PGSE) NMR, coupled with various data processing schemes, is a powerful method for the mixture analysis of D owing to (PGSE) NMR method can easily be applied to measure variable temperature diffusion data simply by changing the temperature of the surrounding the sample tube. Moreover, NMR can afford temperature-dependent spin-lattice relaxation times T_1 for magnetic nuclei such as ^{1}H and ^{13}C atom for the ion.

In the present work, the impact of the addition of lithium salt on viscosity, conductivity, translational diffusion, and molecular motion in lithium bis(trifluoromethanesulfonyl)imide (LiTFSI)-doped 1-methyl-3-pentylimidazolium bis(trifluoromethanesulfonyl)imide [MPI][TFSI] and 1,2-dimethyl-3-pentyl-imidazolium bis(trifluoromethylsulfonyl)amide [DMPI][TFSI] is evaluated. The relationship between the ionic conductivity and the viscosity in the neat [MPI][TFSI], LiTFSI-doped [MPI][TFSI], neat [DMPI][TFSI], and LiTFSI-doped [DMPI][TFSI] is analyzed using the Walden rule. The translational diffusion and rotational motions of neat [MPI][TFSI], LiTFSI-doped [MPI][TFSI], neat [DMPI][TFSI], and LiTFSI-doped [DMPI][TFSI] were investigated by ^{1}H and ^{19}F pulsed field-gradient NMR and ^{13}C spin−lattice relaxation (T_1) measurements, respectively. The HOESY spectra analysis of LiTFSI-doped [MPI][TFSI] and LiTFSI-doped [DMPI][TFSI] is also investigated.

2. EXPERIMENTAL

2.1. Materials and measurement

1-methylimidazole (99 %), 1,2-dimethylimidazole (98%), and 1-bromopentane (99 %) were obtained from Aldrich and used without further purification. Lithium

bis(trifluoromethanesulfonyl)imide (99 %) was purchased from TCI. The conductivity (σ) of the ionic liquid was systematically measured with a conductivity meter LF 340 and a standard conductivity cell TetraCon 325 (Wissenschaftlich-Technische Werkstätten GmbH, Germany). The cell constant was determined by calibration after each sample measurement using an aqueous 0.01 M KCl solution. The density of the ILs was measured with a dilatometer, which was calibrated by measuring the density of neat glycerin at 30, 40, 50, 60, 70, and 80 ^{o}C. The dilatometer was placed in a thermostatic water bath (TV-4000, TAMSON) whose temperature was regulated to within ± 0.01 K. To measure density, IL or a binary mixture was placed into the dilatometer up to the mark, the top of the capillary tube (located on the top of the dilatometer) was sealed, and the dilatometer (with capillary tube) was placed into a temperature bath for 10 min to allow the temperature to equilibrate. The main interval between the two marks in the capillary tube was 0.01 cm^3, and the minor interval between two marks was 0.001 cm^3. From the correction coefficient of glycerin in capillary tube at various temperatures, we can calculate the density of neat IL or binary system by the expanded volume of liquid in the capillary tube at various temperatures. Each sample was measured at least three times to determine an average value, and the values of the density were ±0.0001 g/mL. The viscosities (η) of the ILs were measured using a calibrated modified Ostwald viscometer (Cannon-Fenske glass capillary viscometers, CFRU, 9721-A50) with inner diameters of 1.2 ± 2% mm [45-48]. The viscometer was placed in a thermostatic water bath (TV-4000, TAMSON), in which the temperature was regulated to within ± 0.01 K. The flow time was measured with a stop watch capable of recording to 0.01 s. For each IL, the experimental viscosity was obtained by averaging three to five flow time measurements. The water content of the dried ILs was detected by a Karl–Fischer moisture titrator (Metrohm 73KF coulometer), and the values were less than 100 ppm. NMR spectra of synthesized ILs were recorded on a BRUKER AV300 spectrometer and calibrated with tetramethylsilane (TMS) as the internal reference.

2.2. Synthesis of 1-methyl-3-pentylimidazolium bis(trifluoromethanesulfonyl)imide [MPI][TFSI]

1-bromopentane (208 g, 1.38 mol) was added to a vigorously stirred solution of 1-methylimidazole (102.6 g, 1.25 mol) in toluene (125 mL) at 0 ^{o}C. The solution was heated to reflux at around 110 ^{o}C for 24 hours, and then cooled to room temperature for 12 hours. The toluene was decanted and the remaining viscous oil was washed with ether several times to yield a viscous liquid, which was dried *in vacuo* to give 1-pentyl-3-methylimidazolium bromide ([MPI][Br]) with a yield of approximately 82 %. ^{1}H-NMR (400MHz, D_2O, ppm): δ 0.80 (t, J = 7.1 Hz, 3H, CH_3), δ 1.14-1.33 (m, 4H, CH_2), δ 1.76-1.86 (m, 2H, CH_2), δ 3.84 (s, 3H, CH_3), δ 4.14 (t, J = 7.1 Hz, 2H, CH_2), δ 7.37-7.40 (m, 1H, CH), δ 7.42-7.44 (m, 1H, CH), δ 8.67 (s, 1H, CH). Elemental analysis (%) is found (C, 46.26; H, 7.32; N, 11.97) and calculated (C, 46.36; H, 7.35; N, 12.02) for synthetic [MPI][Br]. An aqueous solution of lithium bis(trifluoromethylsulfonyl)imide (100 mmol, 28.7 g) was then added to an aqueous solution of [MPI][Br] (100 mmol, 23.3 g). The mixture was reacted for 3 h at 60 ^{o}C. After cooling, a white oily product was formed, which was extracted with chloroform. After removing the solvent under reduced pressure, a colorless oily product was obtained. Then, the combined solution was dried in a vacuum at 100 ^{o}C to remove the water. Yield: 91%. ^{1}H NMR (300 MHz, DMSO-d_6, ppm): 8.99 (s,

1H, hydrogen of imidazolium), 7.64 (d, 1H, hydrogen of imidazolium), 7.57 (d, 1H, hydrogen of imidazolium), 4.05 (t, 2H, N–CH_2–), 3.75 (s, 3H, N–CH_3), 1.69 (m, 2H, N–CH_2–CH_2–), 1.22 (m, 2H, N–CH_2–CH_2–CH_2–), 1.13 (m, 2H, N–CH_2–CH_2–CH_2–CH_2–), 0.77 (t, 3H, N–CH_2–CH_2–CH_2–CH_2–CH_3). ^{19}F NMR(400 MHz, DMSO-d_6): 82.8 ppm. Elem. Anal. Calcd. for $C_{11}H_{17}F_6N_3O_4S_2$: C, 30.48%; H, 3.95%; N, 9.70%. Found: C, 30.35%; H, 3.91%; N, 9.58%. The Br^- contents were confirmed with ICP-MS, which was below 0.5% w/w. The structure of [MPI][TFSI] is shown in Fig. 1.

2.3. Synthesis of 1,2-dimethyl-3-pentylimidazolium bis(trifluoromethanesulfonyl)imide [DMPI][TFSI]

[DMPI][Br] was synthesized by a method similar to [MPI][Br]. Yield: 86 %. ^{1}H NMR (300 MHz, D_2O, ppm): 7.23 (d, 1H, hydrogen of imidazolium), 7.20 (d, 1H, hydrogen of imidazolium), 3.99 (t, 2H, N-C$\underline{H}_2$-), 3.65 (s, 3H, N-C$\underline{H}_3$), 2.47 (s, 3H, C-C$\underline{H}_3$), 1.64-1.75 (m, 2H, N-CH_2-C$\underline{H}_2$-), 1.29-1.11 (m, 4H, N-CH_2-CH_2-C$\underline{H}_2$- and N-CH_2-CH_2-CH_2-C$\underline{H}_2$-), 0.76 (t, 3H, N-CH_2-CH_2-CH_2-CH_2-C$\underline{H}_3$). Elem. Anal. Calcd. for $C_{10}H_{19}BrN_2$: C, 48.59 %; H, 7.75 %; N, 11.33 %. Found: C, 48.52 %; H, 7.76 %; N, 11.28 %. [DMPI][TFSI] was prepared by a method similar to [MPI][TFSI]. Yield: 90 %. ^{1}H NMR (300 MHz, DMSO-d_6, ppm): 7.54 (d, 1H, hydrogen of imidazolium), 7.51 (d, 1H, hydrogen of imidazolium), 4.02 (t, 2H, N-C$\underline{H}_2$-), 3.67 (s, 3H, N-C$\underline{H}_3$), 2.50 (s, 3H, C-C$\underline{H}_3$), 1.64 (m, 2H, N-CH_2-C$\underline{H}_2$-), 1.26-1.16 (m, 4H, N-CH_2-CH_2-C$\underline{H}_2$- and N-CH_2-CH_2-CH_2-C$\underline{H}_2$-), 0.80 (t, 3H, N-CH_2-CH_2-CH_2-CH_2-C$\underline{H}_3$). ^{19}F NMR (400 MHz, DMSO-d_6): 82.8 ppm. Elem. Anal. Calcd. for $C_{12}H_{19}F_6N_3O_4S_2$: C, 32.21 %; H, 4.28 %; N, 9.39 %. Found: C, 32.07 %; H, 4.23 %; N, 9.27 %. The Br^- contents were confirmed with ICP-MS, being below 0.5% w/w. The structure of [DMPI][TFSI] is also shown in Fig. 1.

(a) (b)

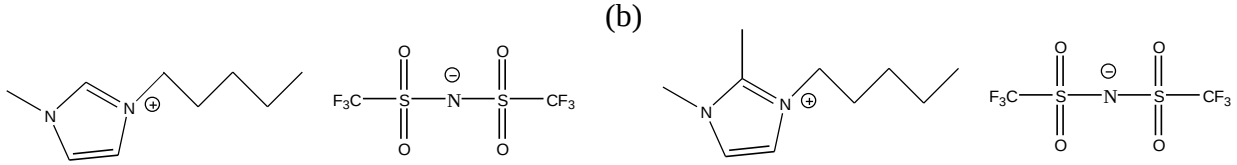

Figure 1. Chemical structure of the studied ionic liquids: (a) 1-methyl-3-pentylimidazolium bis(trifluoromethanesulfonyl)imide [MPI][TFSI]; (b) 1,2-dimethyl-3-pentylimidazolium bis(trifluoromethanesulfonyl)imide [DMPI][TFSI].

2.4. Translational diffusion measurements and molecular motion

A portion of each sample was degassed and sealed in a cylindrical Pyrex tube under high vacuum at room temperature. The sealed sample tube was inserted into a standard 5 mm tube filled with an external lock solvent of D_2O. ^{1}H, ^{19}F, ^{7}Li NMR measurements were carried out on a Bruker Advance 500 with a 5 mm pulsed-field gradient probe. The signals of ^{1}H in $[MPI]^+$ (or $[DMPI]^+$), ^{7}Li in Li^+, and ^{19}F in bis(trifluoromethanesulfonyl)imide anion were used for the determination of self-diffusion coefficients [D_{MPI^+} , D_{DMPI^+} , D_{Li^+} , and D_{TFSI^-}] of the cation and anion species, respectively.

The sample temperature was controlled within ±0.1K by a variable temperature control unit using heated.

Pulsed-gradient spin-echo diffusion measurements were carried out using a stimulated spin-echo sequence. In the pulsed-field gradient spin-echo NMR experiment, the self-diffusion coefficient, *D*, is given by Tanner and Stejskal [46]:

$$\ln\left(\frac{A}{A_0}\right) = -D\gamma^2(\Delta - \frac{\delta}{3})\delta^2 g^2 \qquad (1)$$

where A and A_0 are the signal integrals in the presence and absence of the pulsed-field gradient, respectively, γ is the nuclear magnetogyric ratio, Δ is the interval between the two gradient pulses, δ is the gradient pulse width, and g is the gradient magnitude. In the present experiments, the pulse-field-gradient interval Δ determines the diffusion time and was varied from 20 to 100 ms, δ was set between 3 and 18 ms, and g was set using a suitable strength. The self-diffusion coefficients were measured five or more times at each temperature. The experimental errors in D_{MPI^+}, D_{DMPI^+}, D_{Li^+}, and D_{TFSI^-} were estimated to be less than 3%.

HOESY experiments were measured for detection of NOEs between Li^+ and MPI^+ (or Li^+ and $DMPI^+$). NOESY (ROESY) was recorded for detection of inter-monomeric NOEs of dimeric MPI^+. Relaxation times (T_1) of ^{13}C atoms of neat [MPI][TFSI], LiTFSI-doped [MPI][TFSI] ($x_{[MPI][TFSI]}$ = 0.75), neat [DMPI][TFSI], and LiTFSI-doped [DMPI][TFSI] ($x_{[DMPI][TFSI]}$ = 0.75) were determined using the inversion recovery (180°-τ-90°-Acq.) sequence [47].

3. RESULTS AND DISCUSSION

3.1. Ionic conductivity and viscosity of LiTFSI-doped [MPI][TFSI] and [DMPI][TFSI]

The density (ρ), viscosity (η), and conductivity (σ) of neat [MPI][TFSI], LiTFSI-doped [MPI][TFSI] ($x_{[MPI][TFSI]}$ = 0.75), neat [DMPI][TFSI], and LiTFSI-doped [DMPI][TFSI] ($x_{[DMPI][TFSI]}$ = 0.75) are plotted in Fig. 2-4, the LiTFSI-doped [MPI][TFSI] and LiTFSI-doped [DMPI][TFSI] are liquid at room temperature. Generally, in a narrow range of temperatures, ρ (g cm^{-3}) can be expressed as follows:

$$\rho = a + bT \qquad (2)$$

where a, b, and T are the density at 0 K (g cm^{-3}), the coefficient of volume expansion (g cm^{-3} K^{-1}), and temperature (K), respectively. Linear temperature dependences of the density are shown in Fig. 2 for neat [MPI][TFSI], LiTFSI-doped [MPI][TFSI] ($x_{[MPI][TFSI]}$ = 0.75), neat [DMPI][TFSI], and LiTFSI-doped [DMPI][TFSI] ($x_{[DMPI][TFSI]}$ = 0.75). The best fit parameters of Eq. (2) are summarized in Table 1. As shown in Fig. 2, the density of LiTFSI-doped ILs are larger than those of neat ILs, for instance, LiTFSI-doped [MPI][TFSI] ($x_{[MPI][TFSI]}$ = 0.75, ρ = 1.4899 g cm^{-1} at 30 °C) has higher density

than [MPI][TFSI] without doping LiTFSI (ρ = 1.4056 g cm^{-1} at 30 ^{o}C). In lithium bis(trifluoromethanesulfonyl)imide-doped IL, a more efficient packing and/or attractive interaction occurred when the IL and LiTFSI were mixed. Accordingly, the filling effect of lithium ion in the interstices of ionic liquids contributes to a denser structure. In the other hand, LiTFSI-doped [MPI][TFSI] ($x_{[MPI][TFSI]}$ = 0.75, ρ = 1.4899 g cm^{-1} at 30 ^{o}C) has higher density than that of LiTFSI-doped [DMPI][TFSI] ($x_{[DMPI][TFSI]}$ = 0.75, ρ = 1.4727 g cm^{-1} at 30 ^{o}C), implying the incorporation of methyl group to replace acidic C-2 hydrogen atom of imidazolium cation decreases the intermolecular packing and therefore decreases the density [48].

Table 1. The adjustable parameters of density ($\rho = a + b \cdot T$) for neat [MPI][TFSI], LiTFSI-doped [MPI][TFSI] ($x_{[MPI][TFSI]}$ = 0.75), neat [DMPI][TFSI], and LiTFSI-doped [DMPI][TFSI] ($x_{[DMPI][TFSI]}$ = 0.75).

ILs and LiTFSI-doped ILs	ρ		
	a	$10^4 b$	R^{2a}
neat **[MPI][TFSI]**	1.665	–8.556	0.9999
$x_{[MPI][TFSI]}$ = 0.75	1.770	–9.239	0.9998
neat **[DMPI][TFSI]**	1.649	-8.498	0.9999
$x_{[DMPI][TFSI]}$ = 0.75	1.746	-9.024	0.9998

[a] Correlation coefficient.

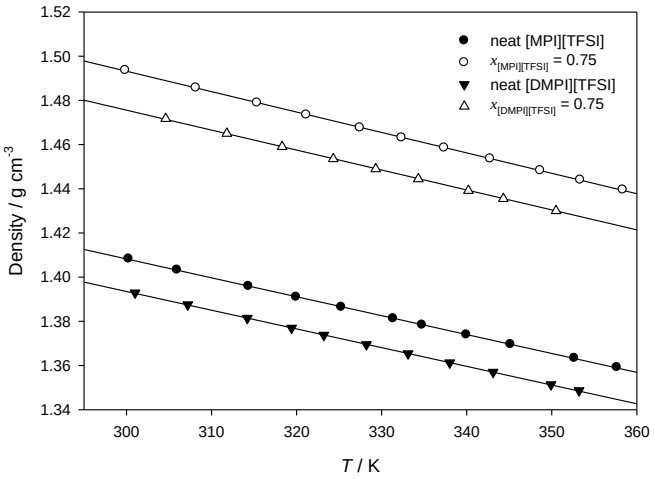

Figure 2. Temperature dependence of density data for neat [MPI][TFSI], LiTFSI-doped [MPI][TFSI] ($x_{[MPI][TFSI]}$ = 0.75), neat [DMPI][TFSI], and LiTFSI-doped [DMPI][TFSI] ($x_{[DMPI][TFSI]}$ = 0.75).

The relative viscosity (Li-salt-doped sample/neat IL sample) is depicted in Fig. 3. In this respect, viscosity of the class of ILs and LiTFSI-doped ILs exhibits a non-Arrhenius temperature dependence even over a short range of temperatures [49]. The viscosity values, η, were fitted using Vogel–Tamman–Fulcher (VTF) equation and modified Vogel–Tamman–Fulcher (modified VTF) equation [50-60]. The modified VTF equation can be expressed as:

$$\eta^{-1} = \frac{\eta_o}{\sqrt{T}} \exp[\frac{-B}{(T - T_o)}] \quad (3)$$

and the VTF equation can be presented as:

$$\eta^{-1} = \eta_o \exp[\frac{-B}{(T - T_o)}] \quad (4)$$

where η_o, B, and T_o are adjustable parameters, the best-fit η_o (mPa s), B (K), and T_o (K) parameters are given in Table 2. The viscosity of neat [MPI][TFSI] < LiTFSI-doped [MPI][TFSI], demonstrating the addition of a Li salt to [MPI][TFSI] increased viscosity due to the enhancement of ion-ion interactions. Moreover, the viscosity of neat [MPI][TFSI] < neat [DMPI][TFSI], this can be attributed to the incorporation of methyl group to replace acidic C-2 hydrogen atom of imidazolium cation increases the van der Waals interactions and therefore increases the viscosity.

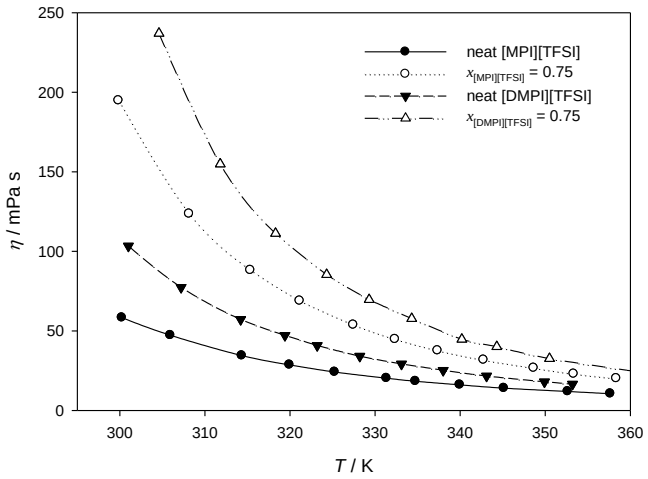

Figure 3. Dynamic viscosity (η) as a function of temperature for neat [MPI][TFSI], LiTFSI-doped [MPI][TFSI] ($x_{[MPI][TFSI]}$ = 0.75), neat [DMPI][TFSI], and LiTFSI-doped [DMPI][TFSI] ($x_{[DMPI][TFSI]}$ = 0.75).

Table 2. The VTF equation parameters of viscosity ($\eta = \eta_o \exp[B/(T - T_o)]$) and conductivity ($\sigma = \sigma_o \exp[-B'/(T - T_o)]$).

ILs and LiTFSI-doped ILs	η				σ			
	η_o / mPa s	T_o / K	B / K	R^{2a}	σ_o / mS cm^{-1}	T_o / K	B' /K	R^{2a}
neat **[MPI][TFSI]**	0.191	164.0	780.3	0.999	21.1	214.9	163.1	0.999
$x_{[MPI][TFSI]}$ = 0.75	0.237	184.1	777.0	0.999	35.7	201.6	341.4	0.999
neat **[DMPI][TFSI]**	0.162	169.0	853.0	0.999	25.1	213.9	226.3	0.999
$x_{[DMPI][TFSI]}$ = 0.75	0.373	200.5	672.1	0.999	21.0	235.5	213.5	0.999

[a] Correlation coefficient.

The temperature dependence of conductivity for neat [MPI][TFSI], LiTFSI-doped [MPI][TFSI] ($x_{[MPI][TFSI]}$ = 0.75), neat [DMPI][TFSI], and LiTFSI-doped [DMPI][TFSI] ($x_{[DMPI][TFSI]}$ = 0.75) is

depicted in Fig. 4. The conductivities of the neat ILs and LiTFSI-doped ILs increase as temperature rises, indicating an increase in temperature results in an increase in the mobility because the viscosity of the liquids is reduced. The observed temperature dependences of conductivity are well fitted by VTF equation:

$$\sigma = \sigma_o \exp[\frac{-B'}{(T - T_o)}] \quad (5)$$

where σ_o, B', and T_o were the fitting parameters, the VTF fitting parameters of the ionic conductivity for these ILs are summarized in Table 2. The conductivity of neat [MPI][TFSI] > neat [DMPI][TFSI] owing to [MPI][TFSI] possesses lower viscosity than [DMPI][TFSI]. On the other hand, the conductivity of ILs decreases upon the addition of LiTFSI into neat ILs and follows the order: (neat [MPI][TFSI]) > ($x_{[MPI][TFSI]}$ = 0.75) and (neat [DMPI][TFSI]) > ($x_{[DMPI][TFSI]}$ = 0.75).

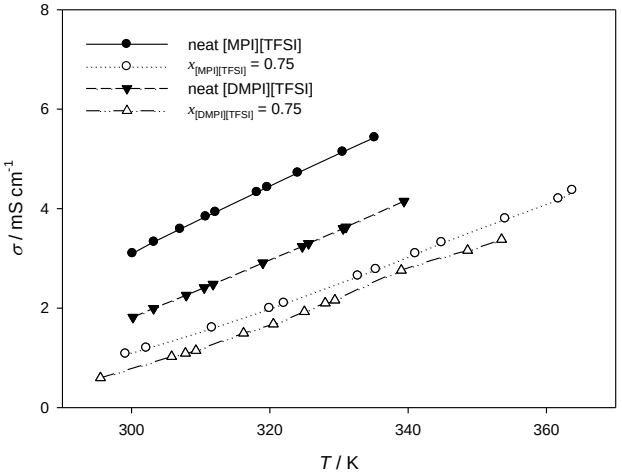

Figure 4. Dependence of specific conductivity (σ) on temperature for neat [MPI][TFSI], LiTFSI-doped [MPI][TFSI] ($x_{[MPI][TFSI]}$ = 0.75), neat [DMPI][TFSI], and LiTFSI-doped [DMPI][TFSI] ($x_{[DMPI][TFSI]}$ = 0.75).

The molar conductivity Λ (S cm^2 mol^{-1}) was obtained by dividing the ionic conductivity by the salt concentration according to the following equation:

$$\Lambda = \sigma \frac{M}{\rho} \quad (6)$$

where M, σ, ρ are the respective equivalent weight, specific conductivity, and density of the ILs. The temperature dependence of Λ for neat [MPI][TFSI], LiTFSI-doped [MPI][TFSI] ($x_{[MPI][TFSI]}$ = 0.75), neat [DMPI][TFSI], and LiTFSI-doped [DMPI][TFSI] ($x_{[DMPI][TFSI]}$ = 0.75) is depicted in Figure 5. The observed temperature dependences of molar conductivity are well fitted by the empirical VTF equation:

$$\Lambda = \Lambda_o \exp[\frac{-B'}{(T - T_o)}] \quad (7)$$

where Λ_o, B', and T_o are the fitting parameters, and VTF fitting parameters of the molar conductivity for the ILs are summarized in Table 3.

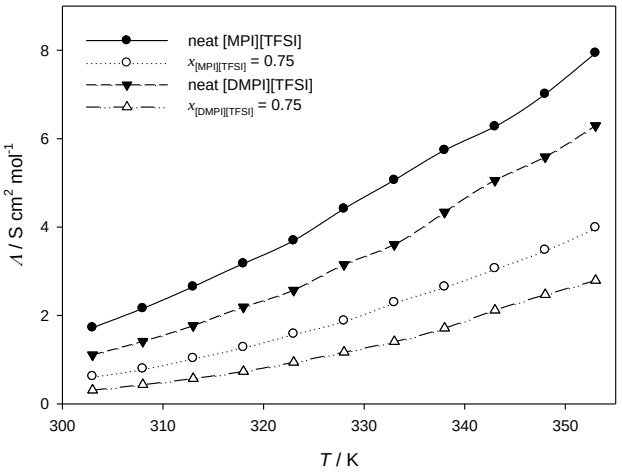

Figure 5. Dependence of molar conductivity (Λ) on temperature for neat [MPI][TFSI], LiTFSI-doped [MPI][TFSI] ($x_{[MPI][TFSI]}$ = 0.75), neat [DMPI][TFSI], and LiTFSI-doped [DMPI][TFSI] ($x_{[DMPI][TFSI]}$ = 0.75).

Table 3. VTF equation parameters of molar conductivity data (Λ = Λ_o exp[-B'/(T - T_o)], Λ_{NMR} = Λ_o exp[-B'/(T - T_o)])

ILs and LiTFSI-doped ILs	Λ				Λ_{NMR}			
	Λ_o / S cm^2 mol^{-1}	T_o/K	B' /K	R^{2a}	Λ_o / S cm^2 mol^{-1}	T_o /K	B' /K	R^{2a}
neat **[MPI][TFSI]**	7.5	210.6	184.1	0.999	110.4	215.9	362.4	0.999
$x_{[MPI][TFSI]}$ = 0.75	11.2	198.3	369.4	0.999	213.7	197.1	618.5	0.999
neat **[DMPI][TFSI]**	9.4	210.5	248.6	0.999	297.6	192.9	615.5	0.999
$x_{[DMPI][TFSI]}$ = 0.75	6.5	233.7	227.5	0.999	180.6	207.6	606.3	0.999

[a] Correlation coefficient.

It has been found that the empirical Walden rule, namely, that molar conductivity is inversely proportional to the viscosity of the medium [61]:

$$\Lambda \eta^{\alpha} = C \quad (8)$$

where C is a temperature-dependent constant, which is called the Walden product. α is the slope of the line in the Walden plot, which reflects the decoupling of the ions. According to the Walden rule, ILs that possess strongly interacting ions in ILs are usually located below the KCl ideal line, due to partial association of neighboring ions. In the present study, neat [MPI][TFSI], LiTFSI-doped [MPI][TFSI] ($x_{[MPI][TFSI]}$ = 0.75), neat [DMPI][TFSI], and LiTFSI-doped [DMPI][TFSI] ($x_{[DMPI][TFSI]}$ = 0.75) are less than the $\Lambda\eta$ of the KCl aqueous solution (Fig. 6), indicating a fraction of ion association in the ILs. Compare the discrepancy from the ideal line of Walden plots, the deviation increases significantly with the addition of LiTFSI to [MPI][TFSI] (or [DMPI][TFSI]), implying the addition of LiTFSI increases the ion association in the IL mixture.

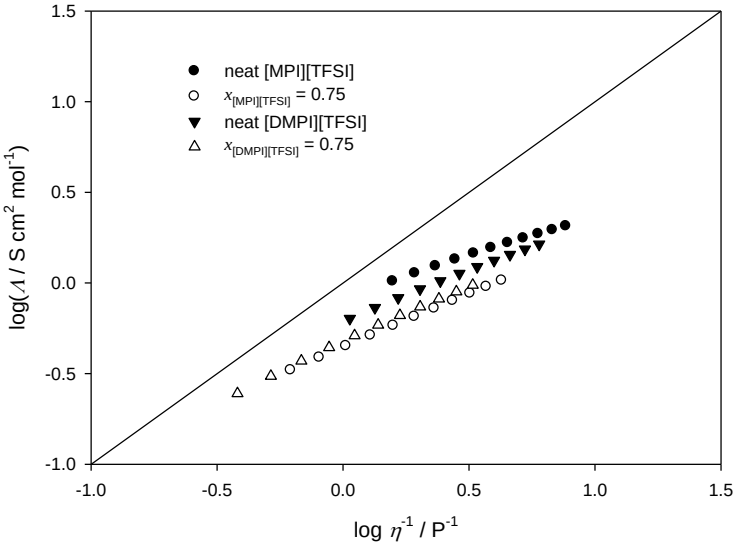

Figure 6. Walden plots for neat ILs and LiTFSI-doped ILs, where Λ is the equivalent conductivity and η^{-1} is the fluidity. The ideal line runs from corner to corner of a square diagram is generated from data obtained in aqueous KCl solution.

3.2. Self-Diffusion Coefficient of the Individual ion

The diffusion coefficients of the ^{1}H, ^{7}Li, and ^{19}F nuclei have been measured for neat [MPI][TFSI], LiTFSI-doped [MPI][TFSI] ($x_{[MPI][TFSI]}$ = 0.75), neat [DMPI][TFSI], and LiTFSI-doped [DMPI][TFSI] ($x_{[DMPI][TFSI]}$ = 0.75). Fig. 7 shows the temperature dependence of the self-diffusion coefficients of the cation (D_{MPI^+}, D_{DMPI^+}, and D_{Li^+}), anion (D_{TFSI^-}), and the summation of the cation and anion ($D_{total} = x D_{Li^+} + (1-x) D_{MPI^+ (or\ DMPI^+)} + D_{TFSI^-}$) for these binary IL solutions, the experimental self-diffusion coefficients D (cm^2 s^{-1}) for neat [MPI][TFSI], LiTFSI-doped [MPI][TFSI] ($x_{[MPI][TFSI]}$ = 0.75), neat [DMPI][TFSI], and LiTFSI-doped [DMPI][TFSI] ($x_{[DMPI][TFSI]}$ = 0.75) are summarized in Table 4. As shown in Fig. 7, some of the temperature dependence curves of $D_{MPI^+ (or\ DMPI^+)}$, D_{Li^+}, D_{TFSI^-} and D_{total} cannot be expressed by a simple linear function. However, the Vogel–Tamman–Fulcher (VTF) equation fits the experimental data very well over the entire temperature range.

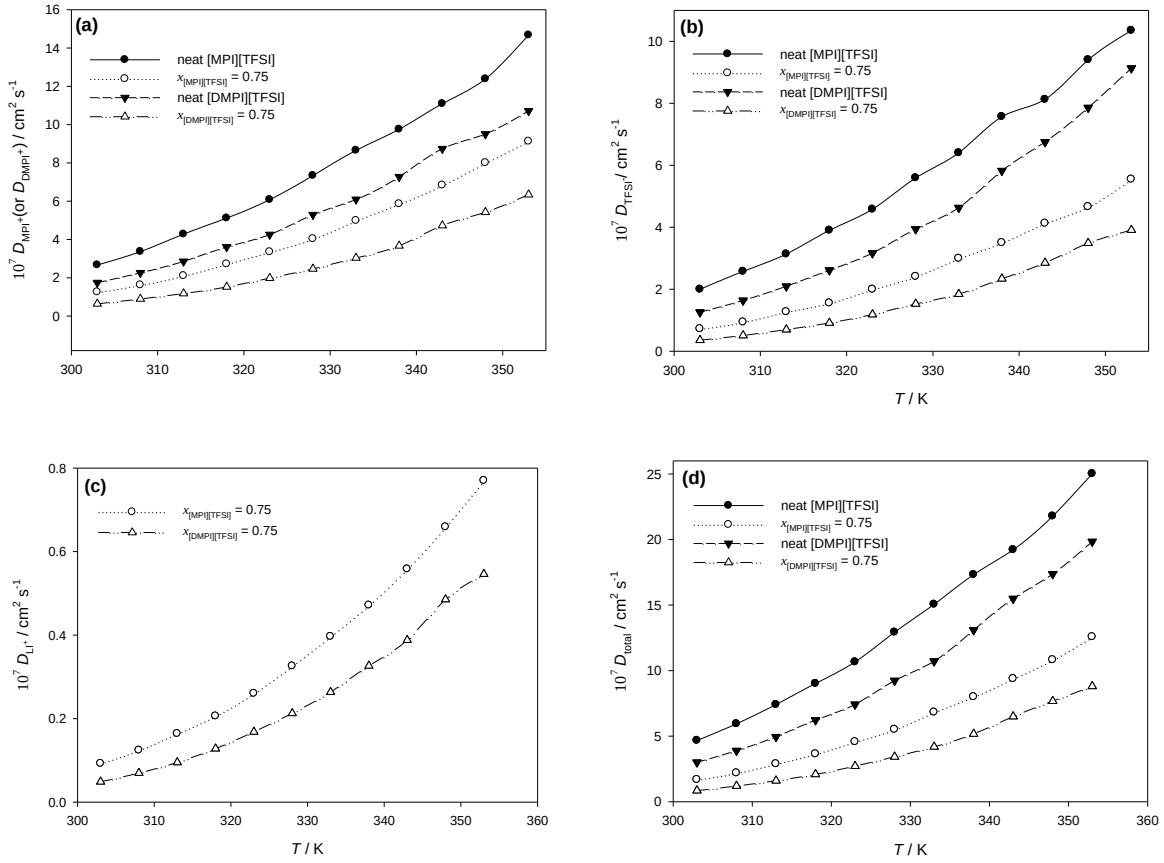

Figure 7. Temperature dependence of the self-diffusion coefficients of ions (a) D_{MPI^+} (or D_{DMPI^+}), (b) D_{TFSI^-}, (c) D_{Li^+}, and (d) D_{total} in neat [MPI][TFSI], LiTFSI-doped [MPI][TFSI] ($x_{[\mathrm{MPI}][\mathrm{TFSI}]}$ = 0.75), neat [DMPI][TFSI], and LiTFSI-doped [DMPI][TFSI] ($x_{[\mathrm{DMPI}][\mathrm{TFSI}]}$ = 0.75).

$$D = D_{\mathrm{o}} \exp[\frac{-B'}{(T - T_{\mathrm{o}})}] \qquad (9)$$

where the constants D_{o} (cm^2 s^{-1}), B (K), and T_{o} (K) are adjustable parameters. The best-fit parameters of the ionic diffusivity are summarized in Table 5 and Table 6, the sum of the cationic and anionic diffusion coefficients (D_{total}) follows the orders: (neat [MPI][TFSI]) > ($x_{[\mathrm{MPI}][\mathrm{TFSI}]}$ = 0.75), (neat [DMPI][TFSI]) > ($x_{[\mathrm{DMPI}][\mathrm{TFSI}]}$ = 0.75), and (neat [MPI][TFSI]) > (neat [DMPI][TFSI]).

Ionic transference numbers at 303.15 K are shown in Table 4 to compare the self-diffusion coefficients of each ion, the ionic transference number t_{i} [62] is defined as:

$$t_{\mathrm{i}} = \frac{x_{\mathrm{i}} D_{\mathrm{i}}}{\Sigma x_{\mathrm{i}} D_{\mathrm{i}}} \qquad (10)$$

The cationic transference number is modified by the addition of LiTFSI, but the Li^+ transference number in LiTFSI-doped IL is very low, close to 0.014. This low t_{Li^+} may be related to (i)

the lower concentration of Li^+ compared to the $TFSI^-$ anion and MPI^+ and $DMPI^+$ cation concentration; (ii) the formation of $[Li(TFSI)_{n+1}]^{n-}$ complexes, leading to an increase of the overall size of the lithium species [63]. Moreover, the ionic transference number of the MPI^+ (or $DMPI^+$) is larger than that of $TFSI^-$ in neat ILs and LiTFSI-doped ILs, and the ionic transference numbers of the MPI^+ (or $DMPI^+$) in neat ILs are larger than those of corresponding LiTFSI-doped ILs.

3.3. Molar conductivity evaluated from the PGSE-NMR diffusion coefficients

The molar conductivity of neat [MPI][TFSI], LiTFSI-doped [MPI][TFSI] ($x_{[MPI][TFSI]}$ = 0.75), neat [DMPI][TFSI], and LiTFSI-doped [DMPI][TFSI] ($x_{[DMPI][TFSI]}$ = 0.75), Λ_{NMR}, is calculated from the self-diffusion coefficients using the expression:

$$\Lambda_{NMR} = \frac{Ne^2(x_{MPI^+(\text{or DMPI}^+)}D_{MPI^+(\text{or DMPI}^+)} + D_{TFSI^-} + x_{Li^+}D_{Li^+})}{kT} \quad (11)$$

where N is the Avogadro number, e is the electric charge on each ionic carrier ($1.602*10^{-19}$ Coulomb), x_{MPI^+} (or x_{DMPI^+}) and x_{Li^+} are the molar ratio of IL and LiTFSI, respectively, k is the Boltzmann constant ($1.38*10^{-23}$), and T is the absolute temperature (K). The temperature dependence of the molar conductivity calculated from the ionic diffusion coefficient and Eq. 11 is shown in Fig. 8 and the best-fit parameters of the VTF equation are listed in Table 3. The experimental molar conductivity value (Λ) is lower than that of the calculated molar conductivity (Λ_{NMR}) over the entire temperature range, implying ion association in ionic liquids [64].

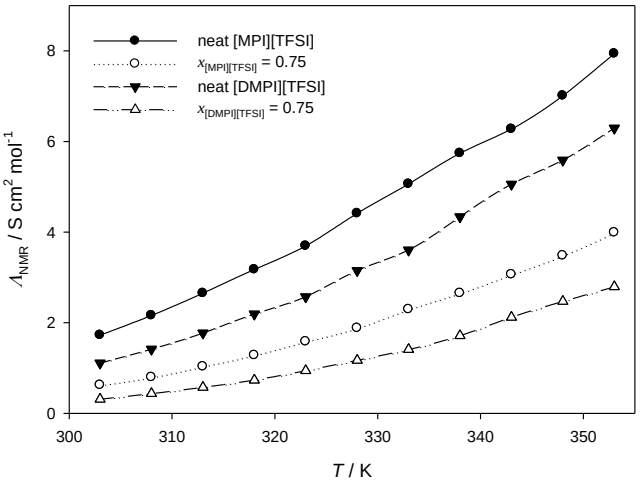

Figure 8. Dependence of molar conductivity (Λ_{NMR}) on temperature for neat [MPI][TFSI], LiTFSI-doped [MPI][TFSI] ($x_{[MPI][TFSI]}$ = 0.75), neat [DMPI][TFSI], and LiTFSI-doped [DMPI][TFSI] ($x_{[DMPI][TFSI]}$ = 0.75). Λ_{NMR} is calculated from PGSE-NMR diffusion coefficient and Nernst-Einstein equation.

Table 4. Experimental self-diffusion coefficients D ($cm^2\ s^{-1}$) and ion transference number t at 303.15 K for neat [MPI][TFSI], LiTFSI-doped [MPI][TFSI] ($x_{[MPI][TFSI]}$ = 0.75), neat [DMPI][TFSI], and LiTFSI-doped [DMPI][TFSI] ($x_{[DMPI][TFSI]}$ = 0.75). Transference number t_i is defined as: $t_i = x_iD_i/\Sigma x_iD_i$.

	ion	D / $cm^2\ s^{-1}$	t
neat **[MPI][TFSI]**	MPI^+	2.67×10^{-7}	0.572
	$TFSI^-$	2.00×10^{-7}	0.428
$x_{[MPI][TFSI]}$ = 0.75	MPI^+	1.26×10^{-7}	0.558
	Li^+	9.25×10^{-9}	0.014
	$TFSI^-$	7.22×10^{-8}	0.429
neat **[DMPI][TFSI]**	MPI^+	1.745×10^{-7}	0.581
	$TFSI^-$	1.258×10^{-7}	0.419
$x_{[DMPI][TFSI]}$ = 0.75	MPI^+	6.373×10^{-8}	0.565
	Li^+	4.866×10^{-9}	0.014
	$TFSI^-$	3.554×10^{-8}	0.420

Table 5. VTF equation parameters of self-diffusion coefficient data ($D = D_o \exp[-B'/(T - T_0)]$) from the MPI^+ of [MPI][TFSI], $DMPI^+$ of [DMPI][TFSI], and $TFSI^-$ of LiTFSI-doped ILs and neat [MPI][TFSI] (or [DMPI][TFSI]).

ILs and LiTFSI-doped ILs	D_{MPI}^+				D_{TFSI}-			
	D_o/$cm^2\ s^{-1}$	T_o (K)	B' (K)	R^{2a}	D_o/$cm^2\ s^{-1}$	T_o (K)	B' (K)	R^{2a}
neat **[MPI][TFSI]**	3.94×10^{-5}	203.8	495.4	0.999	2.12×10^{-5}	212.4	422.5	0.999
$x_{[MPI][TFSI]}$ = 0.75	1.12×10^{-4}	183.9	809.2	0.999	4.83×10^{-5}	194.0	709.8	0.999
neat **[DMPI][TFSI]**	5.06×10^{-5}	198.6	591.7	0.999	1.40×10^{-4}	174.5	901.1	0.999
$x_{[DMPI][TFSI]}$ = 0.75	8.19×10^{-5}	196.2	764.2	0.999	3.29×10^{-5}	210.4	632.1	0.999

[a] Correlation coefficient.

Table 6. VTF equation parameters of self-diffusion coefficient data ($D = D_o \exp[-B'/(T - T_0)]$) from Li^+ of LiTFSI-doped [MPI][TFSI] (or LiTFSI-doped [DMPI][TFSI]), ($MPI^+ + TFSI^- + Li^+$) of (LiTFSI-doped [MPI][TFSI] and neat [MPI][TFSI]), and ($DMPI^+ + TFSI^- + Li^+$) of (LiTFSI-doped [DMPI][TFSI] and neat [DMPI][TFSI]).

ILs and LiTFSI-doped ILs	D_{Li}^+				D_{total}			
	D_o/$cm^2\ s^{-1}$	T_o (K)	B' (K)	R^{2a}	D_o/$cm^2\ s^{-1}$	T_o (K)	B' (K)	R^{2a}
neat **[MPI][TFSI]**	---	---	---	---	5.96×10^{-5}	207.6	462.6	0.999
$x_{[MPI][TFSI]}$ = 0.75	7.85×10^{-6}	193.3	739.4	0.999	1.31×10^{-4}	188.7	761.8	0.999
neat **[DMPI][TFSI]**	---	---	---	---	1.78×10^{-4}	184.8	754.9	0.999
$x_{[DMPI][TFSI]}$ = 0.75	5.29×10^{-6}	209.4	654.2	0.999	9.53×10^{-5}	202.5	705.6	0.999

[a] Correlation coefficient.

Table 7. T_1 values of neat and LiTFSI-doped MPI[TFSI] and DMPI[TFSI] at various ^{13}C chemical shifts at 303.15 K.

	Chemical shift of ^{13}C	**Neat [MPI][TFSI]**	**$x_{[MPI][TFSI]}$ = 0.75**
MPI^+	135.55	0.42	0.32
	123.36	0.39	0.31
	122.06	0.41	0.30
	49.56	0.32	0.22
	35.37	1.16	0.88
	29.15	0.42	0.33
	27.59	0.53	0.44
	21.4	0.93	0.69
	12.64	1.96	1.56
$TFSI^-$	119.47	1.91	0.98
	Chemical shift of ^{13}C	**neat [DMPI][TFSI]**	**$x_{[DMPI][TFSI]}$ = 0.75**
$DMPI^+$	121.97	0.25	0.24
	120.52	0.27	0.22
	48.18	0.23	0.22
	34.27	1.14	1.03
	28.77	0.32	0.29
	27.66	0.45	0.40
	21.52	0.69	0.59
	12.72	1.65	1.49
	12.64	1.96	1.56
$TFSI^-$	119.47	1.91	0.98

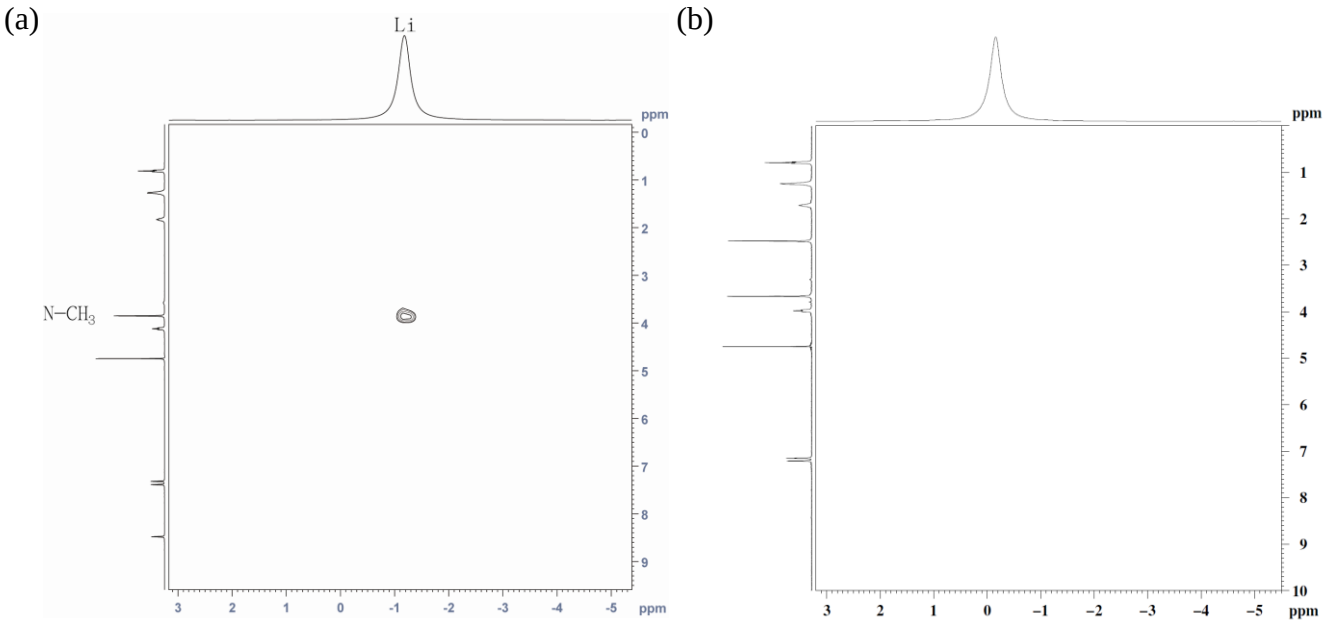

Figure 9. HOESY spectra of (a) LiTFSI-doped [MPI][TFSI] ($x_{[MPI][TFSI]}$ = 0.75) and (b) LiTFSI-doped [DMPI][TFSI] ($x_{[DMPI][TFSI]}$ = 0.75) at 303.15 K.

3.4. Molecular motion

Fig. 9(a) and Fig. 9(b) shows the HOESY spectra of LiTFSI-doped [MPI][TFSI] ($x_{[MPI][TFSI]}$ = 0.75) and LiTFSI-doped [DMPI][TFSI] ($x_{[DMPI][TFSI]}$ = 0.75), respectively, the NOE was assigned to the interaction of Li^+ and N-CH_3 of MPI^+. As shown in Fig. 9(a), LiTFSI-doped [MPI][TFSI] ($x_{[MPI][TFSI]}$ = 0.75) shows a NOE signal between Li^+ and MPI^+ and a broad Li peak was observed, whereas there is no NOE signal in LiTFSI-doped [DMPI][TFSI] ($x_{[DMPI][TFSI]}$ = 0.75) in Fig. 9(b), which indicates that Li^+ prefer to interact with MPI^+ rather than that with $DMPI^+$ in LiTFSI-doped ILs, this can be attributed to one additional methyl group at the C-2 position in the $DMPI^+$ may prevent Li^+ to be closed to $DMPI^+$ via steric hindrance. Fig. 10 shows the inter-monomeric NOEs of LiTFSI-doped [MPI][TFSI], the inter-monomeric NOEs are observed between N-CH_3 and C(terminal) (t-CH_3), and between N-CH_3 and CH_2 of imidazolium. It was reported that MPI^+ can form a dimer in the ion liquid [65], the inter-monomeric NOEs were present between N-CH_3 and C(terminal) (t-CH_3), and between N-CH_3 and CH_2 in LiTFSI-doped [MPI][TFSI], but they can not be observed in neat [MPI][TFSI], demonstrating dimer formation in LiTFSI-doped [MPI][TFSI].

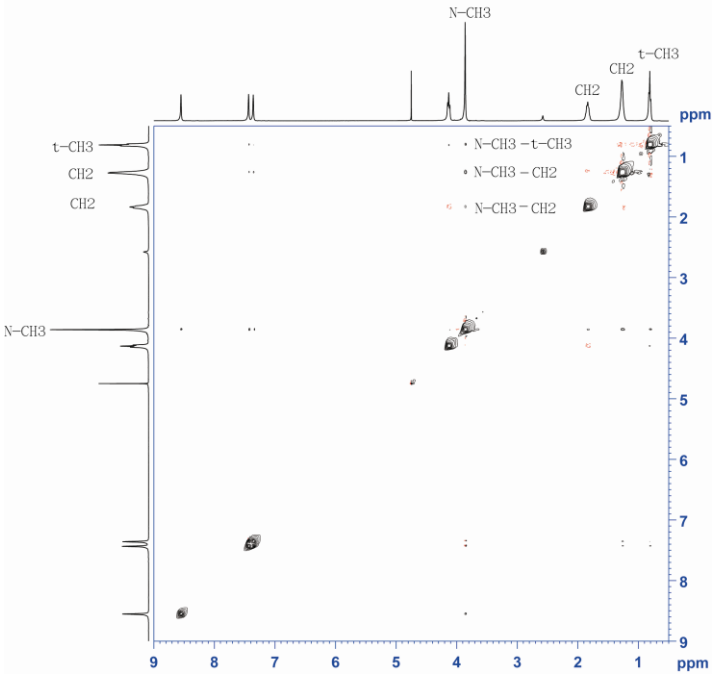

Figure 10. Inter-monomeric NOEs of LiTFSI-doped [MPI][TFSI] ($x_{[MPI][TFSI]}$ = 0.75) at 303.15 K.

In order to investigate the dynamics of neat [MPI][TFSI], LiTFSI-doped [MPI][TFSI] ($x_{[MPI][TFSI]}$ = 0.75), neat [DMPI][TFSI], and LiTFSI-doped [DMPI][TFSI] ($x_{[DMPI][TFSI]}$ = 0.75), T_1 values of ^{13}C atoms in them were measured. Before the addition of lithium salt, the T_1 values of the ^{13}C atoms in the aliphatic side chain decreased gradually from terminal methyl group of pentyl chain to imidazole ring (Table 7), indicating that the terminal group of pentyl chain is more flexible than that of imidazole unit, which is expected from segmental motion. After the addition of LiTFSI, the T_1 values of all ^{13}C atoms decreased (Table 7), this can be attributed to the viscosity of the LiTFSI-doped [MPI][TFSI] is higher than that of neat [MPI][TFSI] at the same temperature. The N-CH_3 group of

imidazole unit in LiTFSI-doped [MPI][TFSI] ($x_{[MPI][TFSI]}$ = 0.75) shows NOE with Li, and the T_1 value decreases from 1.16 s to 0.88 s after the addition of lithium salt, which is still relative longer than other carbons of pentyl chain, except t-CH_3 shows longer T_1 (T_1 = 1.56 s), suggesting that the N-CH_3 rotates rapidly in LiTFSI-doped [MPI][TFSI].

4. CONCLUSIONS

We present a comparative study on the transport properties of neat [MPI][TFSI], LiTFSI-doped [MPI][TFSI], neat [DMPI][TFSI], and LiTFSI-doped [DMPI][TFSI] through conductivity (σ), viscosity (η), and self-diffusion coefficient (D) measurements. The self-diffusion coefficients (D) of the ion species in neat [MPI][TFSI], LiTFSI-doped [MPI][TFSI], neat [DMPI][TFSI], and LiTFSI-doped [DMPI][TFSI] were determined by observing ^{1}H, ^{7}Li, and ^{19}F nuclei with the pulsed-field gradient spin−echo NMR technique, and the transference numbers of $D_{MPI^+ (or\ DMPI^+)}$, D_{Li^+}, D_{TFSI^-} were estimated. Results show that the ionic transference number of the MPI^+ (or $DMPI^+$) is larger than that of $TFSI^-$ in neat ILs and LiTFSI-doped ILs, and the ionic transference numbers of the MPI^+ (or $DMPI^+$) in neat ILs are larger than those of corresponding LiTFSI-doped ILs.

ACKNOWLEDGEMENTS
The authors would like to thank the National Science Council of the Republic of China for financially supporting this project. We are very grateful to Ms. Ru-Rong Wu for her help in performing the NMR experiments.

References

1. R.D. Rogers, K.R. Seddon, Ionic Liquids: Industrial Applications for Green Chemistry, American Chemical Society, Washington, DC, 2003.
2. B. Baek, S. Lee, C. Jung, *Int. J. Electrochem. Sci.,* 6 (2011) 6220.
3. T.Y. Wu, B.K. Chen, L. Hao, K.F. Lin, I.W. Sun, *J. Taiwan Inst. Chem. Eng.*, 42 (2011) 914.
4. N.V. Likhanova, O. Olivares-Xometl, D. Guzman-Lucero, M.A. Dominguez-Aguilar, N. Nava, M. Corrales-Luna, M.C. Mendoza, *Int. J. Electrochem. Sci.,* 6 (2011) 4514.
5. T.Y. Wu, H.C. Wang, S.G. Su, S.T. Gung, M.W. Lin, C.B. Lin, *J. Chin. Chem. Soc.*, 57 (2010) 44.
6. H. Wang, L.X. Wu, Y.C. Lan, J.Q. Zhao, J.X. Lu, *Int. J. Electrochem. Sci.,* 6 (2011) 4218.
7. T.Y. Wu, B.K. Chen, C.W. Kuo, L. Hao, Y.C. Peng, I.W. Sun, *J. Taiwan Inst. Chem. Eng.*, 43 (2012) 860.
8. S.K. Shukla, L.C. Murulana, E.E. Ebenso, *Int. J. Electrochem. Sci.,* 6 (2011) 4286.
9. T.Y. Wu, B.K. Chen, L. Hao, C.W. Kuo, I.W. Sun, *J. Taiwan Inst. Chem. Eng.*, 43 (2012) 313.
10. T.Y. Wu, S.G. Su, Y.C. Lin, H.P. Wang, M.W. Lin, S.T. Gung, I.W. Sun, *Electrochim. Acta,* 56 (2010) 853.
11. H.A. Barham, S.A. Brahim, Y. Rozita, K.A. Mohamed, *Int. J. Electrochem. Sci.,* 6 (2011) 181.
12. T.Y. Wu, I.W. Sun, S.T. Gung, B.K. Chen, H.P. Wang, S.G. Su, *J. Taiwan Inst. Chem. Eng.*, 42 (2011) 874.

13. T.Y. Wu, S.G. Su, K.F. Lin, Y.C. Lin, H.P. Wang, M.W. Lin, S.T. Gung, I.W. Sun, *Electrochim. Acta*, 56 (2011) 7278.
14. P.N. Tshibangu, S.N. Ndwandwe, E.D. Dikio, *Int. J. Electrochem. Sci.,* 6 (2011) 2201.
15. T.Y. Wu, S.G. Su, H.P. Wang, I.W. Sun, *Electrochem. Commun.,* 13 (2011) 237.
16. T.Y. Wu, S.G. Su, S.T. Gung, M.W. Lin, Y.C. Lin, C.A. Lai, I.W. Sun, *Electrochim. Acta,* 55 (2010) 4475.
17. L.C. Xuan, Y.X. An, W. Fang, L.X. Liao, Y.L. Ma, Z.Y. Ren, G.P. Yin, *Int. J. Electrochem. Sci.,* 6 (2011) 6590.
18. Y.X. An, P.J. Zuo, X.Q. Cheng, L.X. Liao, G.P. Yin, *Int. J. Electrochem. Sci.,* 6 (2011) 2398.
19. T.Y. Wu, L. Hao, C.W. Kuo, Y.C. Lin, S.G. Su, P.L. Kuo, I.W. Sun, *Int. J. Electrochem. Sci.,* 7 (2012) 2047.
20. S. Ibrahim, M.R. Johan, *Int. J. Electrochem. Sci.,* 6 (2011) 5565.
21. H. Ganjali, M.R. Ganjali, T. Alizadeh, F. Faridbod, P. Norouzi, *Int. J. Electrochem. Sci.,* 6 (2011) 6085.
22. M.R. Ganjali, H. Ganjali, M. Hosseini, P. Norouzi, *Int. J. Electrochem. Sci.,* 5 (2010) 967.
23. R. Mirshafian, M.R. Ganjali, P. Norouzi, *Int. J. Electrochem. Sci.,* 7 (2012) 1656.
24. M. Pandurangachar, B.E.K. Swamy, B.N. Chandrashekar, O. Gilbert, S. Reddy, B.S. Sherigara, *Int. J. Electrochem. Sci.,* 5 (2010) 1187.
25. P. Norouzi, Z. Rafiei-Sarmazdeh, F. Faridbod, M. Adibi, M.R. Ganjali, *Int. J. Electrochem. Sci.,* 5 (2010) 367.
26. F. Faridbod, M.R. Ganjali, M. Pirali-Hamedani, P. Norouzi, *Int. J. Electrochem. Sci.,* 5 (2010) 1103.
27. M.R. Ganjali, M.H. Eshraghi, S. Ghadimi, S.M. Moosavi, M. Hosseini, H. Haji-Hashemi, P. Norouzi, *Int. J. Electrochem. Sci.,* 6 (2011) 739.
28. M.R. Ganjali, T. Poursaberi, M. Khoobi, A. Shafiee, M. Adibi, M. Pirali-Hamedani, P. Norouzi, *Int. J. Electrochem. Sci.,* 6 (2011) 717.
29. P. Norouzi, M. Hosseini, M.R. Ganjali, M. Rezapour, M. Adibi, *Int. J. Electrochem. Sci.,* 6 (2011) 2012.
30. M.R. Ganjali, M.R. Moghaddam, M. Hosseini, P. Norouzi, *Int. J. Electrochem. Sci.,* 6 (2011) 1981.
31. M.R. Ganjali, M. Hosseini, M. Pirali-Hamedani, H.A. Zamani, *Int. J. Electrochem. Sci.,* 6 (2011) 2808.
32. M.R. Ganjali, M. Rezapour, S.K. Torkestani, H. Rashedi, P. Norouzi, *Int. J. Electrochem. Sci.,* 6 (2011) 2323.
33. P. Norouzi, M. Pirali-Hamedani, S.O. Ranaei-Siadat, M.R. Ganjali, *Int. J. Electrochem. Sci.,* 6 (2011) 3704.
34. F. Faridbod, H.A. Zamani, M. Hosseini, M. Pirali-Hamedani, M.R. Ganjali, P. Norouzi, *Int. J. Electrochem. Sci.,* 6 (2011) 3694.
35. M.R. Ganjali, S.O. Ranaei-Siadat, H. Rashedi, M. Rezapour, P. Norouzi, *Int. J. Electrochem. Sci.,* 6 (2011) 3684.
36. T.H. Tsai, K.C. Lin, S.M. Chen, *Int. J. Electrochem. Sci.,* 6 (2011) 2672.
37. M.R. Ganjali, T. Alizadeh, F. Azimi, B. Larjani, F. Faridbod, P. Norouzi, *Int. J. Electrochem. Sci.,* 6 (2011) 5200.
38. T.Y. Wu, M.H. Tsao, F.L. Chen, S.G. Su, C.W. Chang, H.P. Wang, Y.C. Lin, W.C. Ou-Yang, I.W. Sun, *Int. J. Mol. Sci.,* 11 (2010) 329.
39. S.Y. Ku, S.Y. Lu, *Int. J. Electrochem. Sci.,* 6 (2011) 5219.
40. T.Y. Wu, M.H. Tsao, F.L. Chen, S.G. Su, C.W. Chang, H.P. Wang, Y.C. Lin, I.W. Sun, *J. Iran. Chem. Soc.,* 7 (2010) 707.
41. M.H. Tsao, T.Y. Wu, H.P. Wang, I.W. Sun, S.G. Su, Y.C. Lin, C.W. Chang, *Mater. Lett.,* 65 (2011) 583.

42. T.Y. Wu, M.H. Tsao, S.G. Su, H.P. Wang, Y.C. Lin, F.L. Chen, C.W. Chang, I.W. Sun, *J. Braz. Chem. Soc.*, 22 (2011) 780.
43. I.W. Sun, H.P. Wang, H. Teng, S.G. Su, Y.C. Lin, C.W. Kuo, P.R. Chen, T.Y. Wu, *Int. J. Electrochem. Sci.*, 7 (2012) 9748.
44. J. Gao, J.G. Liu, W.M. Liu, B. Li, Y.C. Xin, Y. Yin, Z.G. Zou, *Int. J. Electrochem. Sci.*, 6 (2011) 6115.
45. A. Fernicola, F. Croce, B. Scrosati, T. Watanabe, H. Ohno, *J. Power Sources*, 174, (2007) 342.
46. J.E. Tanner, E.O. Stejskal, *J. Chem. Phys.*, 49 (1968) 1768.
47. E. Fukushima, S.B.W. Roeder, *Experimental Pulse NMR: A Nuts and Bolts Approach*; Addision-Wesley Publishing Company: Reading, MA, 1981.
48. T.Y. Wu, S.G. Su, S.T. Gung, M.W. Lin, Y.C. Lin, W.C. Ou-Yang, I.W. Sun, C.A. Lai, *J. Iran. Chem. Soc.*, 8 (2011) 149.
49. K.R. Seddon, A.S. Starck, M.J. Torres, ACS Symposium Series 901, Washington, DC, 2004.
50. T.Y. Wu, B.K. Chen, L. Hao, Y.C. Peng, I.W. Sun, *Int. J. Mol. Sci.*, 12 (2011) 2598.
51. T.Y. Wu, B.K. Chen, L. Hao, Y.C. Lin, H.P. Wang, C.W. Kuo, I.W. Sun, *Int. J. Mol. Sci.*, 12 (2011) 8750.
52. I.W. Sun, Y.C. Lin, B.K. Chen, C.W. Kuo, C.C. Chen, S.G. Su, P.R. Chen, T.Y. Wu, *Int. J. Electrochem. Sci.*, 7 (2012) 7206.
53. T.Y. Wu, H.C. Wang, S.G. Su, S.T. Gung, M.W. Lin, C.B. Lin, *J. Taiwan Inst. Chem. Eng.*, 41 (2010) 315.
54. T.Y. Wu, I.W. Sun, S.T. Gung, M.W. Lin, B.K. Chen, H.P. Wang, S.G. Su, *J. Taiwan Inst. Chem. Eng.*, 42 (2011) 513.
55. C.W. Kuo, C.W. Huang, B.K. Chen, W.B. Li, P.R. Chen, T.H. Ho, C.G. Tseng, T.Y. Wu, *Int. J. Electrochem. Sci.*, 8 (2013) 3834.
56. T.Y. Wu, S.G. Su, H.P. Wang, Y.C. Lin, S.T. Gung, M.W. Lin, I.W. Sun, *Electrochim. Acta*, 56 (2011) 3209.
57. T.Y. Wu, I.W. Sun, M.W. Lin, B.K. Chen, C.W. Kuo, H.P. Wang, Y.Y. Chen, S.G. Su, *J. Taiwan Inst. Chem. Eng.*, 43 (2012) 58.
58. C.W. Kuo, W.B. Li, P.R. Chen, J.W. Liao, C.G. Tseng, T.Y. Wu, *Int. J. Electrochem. Sci.*, 8 (2013) 5007.
59. T.Y. Wu, L. Hao, P.R. Chen, J.W. Liao, *Int. J. Electrochem. Sci.*, 8 (2013) 2606.
60. T.Y. Wu, L. Hao, P.R. Chen, J.W. Liao, *Int. J. Electrochem. Sci.*, 8 (2013) 5067.
61. M. Yoshizawa, W. Xu, C.A. Angell, *J. Am. Chem. Soc.*, 125 (2003) 15411.
62. F. Castiglione, E. Ragg, A. Mele, G.B. Appectecchi, M. Montanino, S. Passerini, *J. Phys. Chem. Lett.*, 2 (2011) 153.
63. Y. Saito, T. Umecky, J. Niwa, T. Sakai, S. Maeda, *J. Phys. Chem. B*, 111 (2007) 11794.
64. H. Tokuda, K. Hayamizu, K. Ishii, M.A.B.H. Susan, M. Watanabe, *J. Phys. Chem. B*, 109 (2005) 6103.
65. G.H. Lane, *Electrochim. Acta*, 83 (2012) 513.